Assessment of tamping-based specimen preparation methods on static liquefaction of loose silty sand

Zhehao Zhu, Feng Zhang, Jean Claude Dupla, Jean Canou, Evelyne Foerster, Qingyun Peng

Assessment of tamping-based specimen preparation methods on static liquefaction of loose silty sand

Zhehao Zhu[a,b], Feng Zhang[a*], Jean-Claude Dupla[a], Jean Canou[a], Evelyne Foerster[b], Qingyun Peng[a]

[a]Ecole des Ponts ParisTech, Laboratoire Navier/CERMES, 6-8 av. Blaise Pascal, 77455 Marne La Vallée cedex 2, France

[b]Commissariat à l'énergie Atomique, DEN, DANS, DM2S, Université Paris-Saclay, F-91191 Gif-sur-Yvette, France

***Corresponding Author:**
Feng Zhang
Ecole des Ponts ParisTech
Laboratoire Navier/CERMES, 6-8 av. Blaise Pascal, 77455 Marne La Vallée cedex 2, France
Email: feng.zhang@enpc.fr

Abstract

Dry and moist tamping methods are widely used for the investigation of sandy soil liquefaction. However, the effect of these two tamping-based reconstitution methods on composite soil liquefaction behavior have been rarely assessed. In this study, the dry and moist tamping methods were assessed using loose silica sand matrix (HN31) containing various amounts of non-plastic silt particles (C500), and by performing a series of undrained triaxial compression tests. Microstructural observations using a high-resolution optical microscope were also performed on loose silty sand specimens that had the similar initial states to those for the undrained triaxial tests. Triaxial results show that for silty sand specimens prepared by dry tamping method, a global dilatant behavior was observed and the undrained shear strength decreased as the fraction of silt particles increased. By contrast, a total reversed phenomenon was observed for those prepared by moist tamping method: all specimens showed more or less limited liquefaction behavior and silt particles mitigated the contractive tendency, which provided beneficial contribution to the undrained shear strength. Microstructural observations show that in the dry tamping method, overall structure formed by the host sand and silt particles was regularly deposited, promoting a more stable strain-hardening response. Moreover, some silt particles were found to be located near sand-sand contact points, significantly loosening the sand matrix. On the contrary, by using moist tamping method, the sand was uniformly covered by bulked silt particles, and the aggregated sand formed the metastable structure, facilitating the occurrence of static liquefaction. Moreover, with the increase of fines fraction, this metastable structure was weakened, characterized by the filling of large inter-sand voids, leading to the increase of undrained shear strength. Thus, a critical value of total fines fraction F_c^{Tot} equalling to 21% was determined, which theoretically verified the insignificant effect of specimen preparation methods on the undrained shear strength. In that case, the metastable structure in specimen prepared by moist tamping method was expected to disappear and the overall response of specimen changed from the dominance of host sand to that of fines.

Keyword: Dry and moist tamping methods, silty sand, undrained triaxial compression test, microstructural observation

1. Introduction

Research activities in clean sand liquefaction have been initiated since the occurrence of two destructive earthquakes in Alaska (United States) and Niigata (Japan) in 1964 that caused tremendous disasters. Substantial understandings of liquefaction characteristics reported in the literature, whether subjected to monotonic or cyclic loadings, are mainly based on reconstituted specimens in triaxial apparatus in laboratory research. As for clean sand, it was found that relative density and confining pressure were two determinant indicators incorporated in the framework of state parameter to delineate between liquefiable and non-liquefiable deposits [1–5]. More importantly, while fixing the test conditions (e.g., relative density and confining pressure) using the same materials, the preparation methods (e.g., dry and moist tamping methods) have also significant effect on liquefaction characteristics: the moist tamping facilitates the occurrence of liquefaction due to the formation of metastable structure, whilst no risk of flow liquefaction by dry tamping due to the absence of metastable structure [6–11].

Nevertheless, a large number of in-situ investigations showed that liquefied sand layer usually contained some fine particles [12,13], especially non-plastic silt content. This explains why, in laboratory research, the impact of fine particles based on distinct specimen preparation methods (e.g., dry and moist tamping methods) did draw numerous attentions. It was found that with the addition of fines at low fraction, the liquefaction resistance could either increase [14–18] or decrease [19–21]. Attempts were made to explain the above controversial phenomena from the plasticity index, grain shape and gradation characteristic of the added fines, as well as the relative mean size of fine particles to that of host sand [22–25]. In the case of sand-fines specimens prepared by moist tamping method, Pitman [15] reported that the liquefaction resistance of Ottawa reference sand was enhanced by adding both plastic Kaolinite and non-plastic crushed quartz particles, which is also consistent with the conclusions drawn by other researchers that the undrained shear strength of specimens formed in submerged condition increased with the increase of fines fraction [14,16–18]. On the contrary, in dry condition, Zhu [25] examined the liquefaction of loose HN31 sand mixed with plastic Kaolinite/Illite particles and non-plastic Silt particles, and observed that the presence of fines reduced the undrained

shear resistance in all cases and a good correlation existed between mean diameter ratio (D_{50}/d_{50}, D_{50} and d_{50} represent the mean diameters of the HN31 sand and added materials, respectively) and undrained shear strength ($S_u=q_{max}/2$). Similar conclusions about this adverse impact of fine particles in dry condition have been repeatedly obtained by others [19–21]. Moreover, Wood [26] performed undrained compression tests on Nevada Sand containing non-plastic silt by altering specimen preparation methods (e.g., tapped funnel deposition, water sedimentation, slurry deposition, mixed dry deposition and air pluviation). With respect to uniformity, visual segregation between the host sand and silt was observed for specimens formed by water sedimentation and air pluviation. Furthermore, the effect of depositional method was reported to be a function of density index: (i) more significant for specimens especially at lower densities; (ii) less important for specimens at higher densities. In its accompanying paper, Yamamuro [27] discussed the effect of two depositional methods (between dry funnel and water sedimentation) on the corresponding microstructure and experimentally found that (i) specimens formed by dry funnel deposition were more prone to liquefaction; (ii) whilst, specimens formed by water sedimentation were much more stable upon shearing. As fines fraction increased, a reasonable explanation was proposed in conjunction with a special procedure allowing the microstructure to be quantitively analyzed: in dry funnel method, specimens contained a higher percentage of unstable grains contacts as compared with those formed by water sedimentation method [27]. To the authors' knowledge, the role of added fines to undrained shear strength is quite different in distinct preparation methods, as well as whether the metastable structure can be formed under the effect of fines in moist condition (as for clean sand), have not been well understood yet, and further investigation is thus needed. From practical and academic points of view, clarifying the role of fine particles in two commonly used tamping-based specimen preparation methods (e.g., dry and moist tamping methods) would be also helpful to well understand the mechanism behind in different methods.

In this study, a series of undrained triaxial tests was performed on loose silty sand specimens prepared by dry and moist tamping methods at different fines fractions. Microstructural observations using a high-resolution optical microscope were also performed on loose silty sand specimens that had the similar initial states to one of the specimens prepared for the undrained triaxial tests, allowing the

mechanism behind, as well as the different roles of fines to be identified in dry and moist tamping methods.

2. Materials and methods

2.1. Materials

All tests in this experimental programme were performed on a commercially available reference sand named Huston 31 (HN31) with a mean grain size D_{50} = 0.35 mm and a specific gravity of G_s = 2.65. The added material is a non-plastic silt flour: C500 with a mean grain size d_{50} = 0.006 mm and a specific gravity of G_s = 2.65. Note that the HN31 host sand and C500 silt have very similar colours: grey-white for HN31 and white for C500 since they are both primarily composed of quartz (S_iO_2>99%). The grain size distribution curves measured by laser diffraction is shown in Fig. 1. The principle of the method is that while passing through a laser beam, a particle could scatter the light at a certain angle and intensity that related to its grain size [23]. Detailed index properties of the used materials are tabulated in Table 1.

The maximum void ratios (e_{max}) of HN31-C500 mixture at each fines fraction were determined, in air-dried state, by using a funnel to introduce well-mixed soil into a constant volume container. Note that, during this procedure, the falling rate needed to be as slow as possible in order to achieve a low-energy deposition in which a loosest configuration could be attained. As for minimum void ratios (e_{min}) that represent the possible densest compacting configuration, the well-mixed soil was introduced into a hand-held container in air-dried state and then subjected to alternative mechanical vibrations (at the bottom of the container above a vibratory table). When no further settlement occurred, the corresponding value could be calculated by postulating that the theorical densest state has been practically achieved. Fig. 2 presents e_{max}, e_{min} versus the total fines fraction (F_c^{Tot}=(m_{C500}/(m_{C500}+m_{HN31}))·100%) determined on air-dried HN31-C500 mixtures [18], where m_{C500}, m_{HN31} stand for the dry mass of added C500 silt and host HN31 sand, respectively. As for e_{min} in connection with the densest state of composite soil, two phenomena can be identified in Fig. 2: (i) with the initial addition of fine particles, e_{min} decreased; (ii) with the further addition of fine particles,

especially after a threshold value, e_{min} tended to gradually increase [28]. This is because at low fines fraction, sand skeleton was formed and coarse sand grains remained in contact with each other. In that case, fine particles primarily filled the skeleton voids (see Fig. 3a), resulting in the decrease in e_{min}. By contrast, at higher fines fraction, sand grains started to disperse in fines matrix (see Fig. 3b), resulting in the increase in e_{min} [28]. The characteristic value F_c^{Tot} (about 19% for HN31-C500) in Fig. 2 was defined as the "transitional fines fraction" (TFC), at which the main soil matrix changed from sand-dominance to fines-dominance [16,29]. On the contrary, as for e_{max} representing the possible loosest state in connection with the liquefaction collapsibility analysis, the curve steadily increased without any drop [30,31]. This suggests that at this extremely loose state, a majority of added fines loosened the sand matrix by separating coarse sand grains (loosening effect) instead of preferentially filling the large skeleton empty voids (densifying effect) as observed in the evolution of e_{min} in the case of F_c^{Tot} smaller than 19%. It should be mentioned that some investigators (including [28,32–34]) experimentally observed an initial declining tendency of e_{max}, very similar to the e_{min}. This is probably related with (i) gradation parameters of test material [28,32]; and (ii) different experimental methodologies for extreme void ratio (e_{min} and e_{max}) determination [33].

2.2. Depositional method

Several well-documented earthquakes suggested that, at liquefied site, the silt particles commonly existed with limited percentage [12,35]. It can be logically deduced that the silty sand is still dominated by coarse sand but polluted by a small quantity of fines. In that case, the impact of low percentage non-plastic silt particles is then of major interest while assessing the liquefaction collapsibility of loose silty sand. For this purpose, the void ratio of sand matrix (see Fig. 4a) instead of global void ratio (see Fig. 4b) was considered as controlled parameter in the preparation stage by adopting the density index of sand matrix [18,36]: $I_{Dmat}=(e_{max}-e_{mat})/(e_{max}-e_{min})$, where e_{mat} is the void ratio of sand matrix and e_{max}, e_{min} represent the maximum and minimum void ratios of clean HN31 sand [37], respectively. A clear benefit of this concept is the ability to keep the quantity of sand forming the global soil matrix exactly constant, irrespective of the fines fraction (see Fig. 4a). It

should be mentioned that density index of sand matrix has been also termed “sand skeleton void ratio” by Polito [38] and Dash [39]. A loosest state of I_{Dmat}=0.00 (or e_{mat}=1.00) favouring liquefaction collapsibility analysis was selected in the present work. The fines fraction (F_c=(m_{C500}/m_{HN31})·100%) was defined as the dry mass of added fines divided by that of the host sand matrix.

2.2.1 Tamping-based specimens preparation methods

Dry tamping

Air pluviation is a common technique to prepare uniform loose specimens for liquefaction collapsibility analysis [37]. However, air pluviation of well-graded soil is not as successful as that of poorly graded soil. This is because the well-graded soil such as binary silty sand (e.g., D_{50}>>d_{50}) may become significantly segregated when deposited by pluviation through air, as coarse grains fall faster than fine particles [40]. In order to overcome this non-uniform problem, dry tamping was thus adopted as an alternative. The silty sand specimens (100 mm in diameter and 200 mm in height) were prepared by 10 layers. In each layer, two materials were mixed by shaking in an enclosed container. Afterwards, they were carefully introduced into a membrane-lined spilt mould by spooning. During this operation, particular attention should be paid to minimize the particles drop height in order to: (i) reduce the potential energy as much as possible to create very loose specimens; (ii) avoid any possible segregation between coarse and fine grains during freefall. It is worth noting that, although extreme attempts were made in this method, it was still difficult to create silty sand specimens with extremely low fines fraction (e.g., F_c<3.5%) in very loose state. This is because the composite soil layer after spooning did not fairly satisfy the thickness requirement (2 cm in height for each layer) for further compaction. Thus, 3 relatively high fines fractions were selected: 5%, 10% and 15%. The good repeatability of this dry tamping method has been reported by Zhu [25] who performed the two parallel undrained triaxial tests with the addition of either plastic (Speswhite) or non-plastic (C500) fines, as well as by Jradi [17], who performed both monotonic and cyclic triaxial tests on NE34 sand-Speswhite mixtures.

187 Moist tamping

188 Moist tamping has been widely employed in many experimental investigations of liquefaction
189 [2,6,9,15–17]. This method provides a clear benefit: it is readily able to create very loose specimens
190 with capillary force, which is viewed as beneficial particularly in liquefaction analysis, where
191 extremely contractive responses are desirable. As for composite soil in this research, the technique
192 consisted of mixing the sand and silt particles in a large blender in partially submerged condition
193 created by adding 5% water (by weight) to the total dry mass. The total mixtures were afterwards
194 divided into 10 layers to fabricate a triaxial specimen of 100 mm in diameter and 200 mm in height.
195 Each layer was consecutively poured in a membrane-lined spilt mould and compacted to a required
196 thickness (2 cm) using a hand-held tamper before the next layer was placed. Note that, while keeping
197 sand matrix unchanged with the gradual addition of fine particles, the latex membrane did not allow
198 very strong compaction effect. Thus, 5 relatively low fines fractions were respectively selected: 0%,
199 1%, 2.5%, 5% and 10%.

200

201 2.2.2. Summary of other sandy specimen preparation methods

202 Dry funnel deposition

203 Owing to the practical convenience, dry funnel deposition is another common technique to prepare
204 silty sand specimens in laboratory research [3,32,41]. The composite soil (after mixing either in
205 blender or by spoon) is placed into a large funnel, which is afterwards slowly raised in the split mould
206 along the specimen axis of symmetry. The movement of the funnel needs to be minimized (similar to
207 dry tamping method) in order to cancel the freefall of composite soil, which eventually leads to the
208 segregation phenomenon. Specimen of higher density could be achieved by means of (i) tapping the
209 split mould in a symmetrical pattern; (ii) raising the funnel more quickly (still without a drop height
210 [26]).

211

Slurry deposition

For the purpose of mimicking a natural fluvial or hydraulic fill deposit and of overcoming inherent problem related to segregation phenomenon, an innovant technique called the slurry deposition method has been develop by Kuerbis [40] and Carraro [42] since the method is capable to reconstitute exceptionally homogeneous specimens in terms of void ratio and particles size gradation, regardless of fines fraction. Slurry deposited specimens are firstly boiled (e.g., in a flask the night before testing) in order to achieve a fully saturated condition. Afterwards, a special mixing tube is needed prior to the placement of soil [26] rather than directly depositing soil into the split mould. After this mixing tube is filled with de-aired water, the flask containing the boiled soil is inverted and lowered through a top central hole of the mixing tube to introduce the soil by removing the cap of the flask. A series of small rotations (about one hour) is indispensable to the mixing tube during this process to create a uniform distribution. In the final step, the triaxial cell base and split mould are respectively installed onto the mixing tube, and the mixing tube could then be carefully removed leaving the sandy specimen in the split mould with the aid of an extension component (on the mixing tube) [26]. It is worth noting that sandy specimens are initially prepared in a very loose state, and uniformly densified specimens could be obtained by inducing mechanical vibration.

Water sedimentation

In water sedimentation method, sandy specimen is initially put in a large flask half filled with water, which is then boiled (similar to slurry deposition method) in order to remove undesirable air bubbles and latter filled up with de-aired water. Prior to placing sandy specimen into split mould: (i) the mould and all drainage lines connecting to specimens need to be seriously saturated by de-aired water; (ii) the capped flask needs to be thoroughly rotated in order to achieve a satisfactory homogeneity. The flask is then inverted and lowered as much as possible to the bottom of the split mould. While the specimen is still located in the split mould, mechanical vibration is a common way to achieve higher density [3,43].

3. Triaxial tests programme

In this study, the specimens were prepared by two tamping-based methods (the dry and moist tamping methods); once the specimens had been formed, the top base was placed and carefully sealed with two O-rings. A slight vacuum between 15-20 kPa was then applied to prevent specimen collapse while removing the split mould, as well as to check the leakage of fragile latex membrane. The saturation of the specimens was carried out as a three-steps process. Firstly, the carbon dioxide (CO_2) was percolated through the specimen for about 15 min in order to replace the air since CO_2 dissolved much more easily in water. Secondly, de-aired water was flushed to saturate the specimens. It should be noted that the flux of CO_2 gas and de-aired water were controlled as low as possible in order not to disturb the soil structure during the saturation phase. Finally, the confining pressure and back pressure were increased in equal incremental step of 20 kPa, until they were respectively equal to 300 kPa and 200 kPa. In all tests, the Skempton's B value ($B=\Delta u/\Delta\sigma_{conf}$) was equal to or greater than 0.98. This value was believed to be high enough to achieve full saturation of sandy soil. Afterwards, drainage valves were closed and the specimen was sheared at a constant rate of 0.5%/min in axial strain (ε_a). The equilibrium of pore water pressure during shearing was verified by the measurements at both top and base parts of specimen. All tests were generally terminated after the axial strain reached about 20% and performed at a controlled ambient temperature of 20 ± 1 ºC. The q_{max} was defined as the maximum shear strength during the axial strain range of 0-20%. Note that, the axial load was measured using an internal load cell to eliminate the need to consider any ram friction that may remarkably affect the measurement of deviator stress especially in terms of liquefaction study of loosely prepared sandy soil. Details of the triaxial tests are summarized in Table 2. Note that identical tests are also included in two companion papers [18,25], respectively.

4. Microstructural tests programme

As mentioned previously, the colours of two test materials (grey-white and white) are highly similar due to the similar mineral composition ($Si0_2$>99%). In that case, it seems difficult to distinguish the coarse and fine particles, especially in relatively small scale. Hence, for the purpose of distinction, the

HN31 sand was, in particular, dyed blue using a commercially available colorant (Basacid Blue 762 liquid supplied by BASF), as shown in Fig. 5. Afterwards, fresh dyed sand was carefully placed in a huge oven for more than an hour at a constant temperature of 105 ºC to further maintain its colour. Finally, the grain size distribution curve of coloured HN31 sand was roughly re-measured by classic dry-sieving, and results showed that neither particles size change nor sand grain aggregation occurred during the dyeing procedures described above.

In order to represent as much as possible the initial fabric of silty sand specimens corresponding to the one of specimens installed into the triaxial apparatus before the saturation phase, the composite soil was deposited in a cylindrical cup of 70 mm in diameter and 14 mm in height (see Fig. 6a) by dry and moist tamping methods, respectively. Microstructural observations were performed using a high-resolution optical microscope (see Fig. 6b). Due to the intrinsic constraints in two reconstitution methods as mentioned previously, microstructural observations were only performed on two fines fractions: 5% and 10%.

5. Triaxial test results

Fig. 7 schematizes the triaxial tests of silty sand specimens reclaimed by dry tamping method at three fines fractions. The evolution of q described in Fig. 7a shows that (i) all the three curves monotonically rase without any downward tendency, showing an extremely strong dilatant behavior; (ii) after the initial increase in pseudo-elastic stage (ε_a<0.5% [18]), q almost linearly increased till the end of test (q_{max} at ε_a=20%). In addition, the deviator stress decreased with the increase of fines fraction, which could serve as evidence that the addition of fine particles changed the overall soil mechanical response. As for evolution of Δu identified in Fig. 7b, after a very short contractive phase ($\dot{\Delta u} > 0$), all specimens were characterized by a remarkable dilatant phase ($\dot{\Delta u} < 0$) where the dissipation of Δu became increasingly important as the fines fraction decreased. The above two phenomena suggest that: (i) the collapsibility of silty sand specimens reconstituted in dry state was very low; (ii) the increase in fines fraction could, to some extent, increased the collapsibility potential.

Fig.8a shows the evolution of deviator stress (q) against axial strain (ε_a) of silty sand specimens reclaimed by moist tamping method. In the case of clean sand specimen (F_c=0%), the q firstly increased and then significantly decreased after a peak value, exhibiting a very strong liquefaction collapsibility potential. By contrast, in the cases of silty sand at F_c=1%, 2.5%, 5% and 10%, the specimens could re-gain the undrained shear resistance after a short-lived temporary reduction and this beneficial phenomenon became much more conspicuous at higher fines fractions, indicating that the addition of fine particles mitigated the strain-softening collapsibility. Regarding the evolution of excess pore water pressure against axial strain identified in Fig. 8b, it can be observed that, for clean sand specimen (F_c=0%), Δu increased continually and reached the highest value Δu_{max} of about 98 kPa at the end of test, exhibiting a pure contractive response. By contrast, for silty sand specimens at F_c=1%, 2.5%, 5% and 10%, all Δu tended to decrease after a peak value Δu_{max}, showing a dilatant response. Thus, the role of added silt fines could be distinguished in two stages: (i) before Δu_{max}, the increase in fines fraction inhibited the fast generation of Δu; (ii) after Δu_{max}, the increase in fines fraction facilitated the dissipation of Δu. The above two phenomena proved that, the response of clean sand reclaimed by moist tamping method was liquefiable with a comparatively high collapsibility potential, but with the addition of fines, silty sand became much less collapsible. Also, the above results (moist tamping method) are opposite to the phenomena observed in Fig. 7a for specimens that were reclaimed by dry tamping method, suggesting that the specimen preparation method has a significant effect on the static liquefaction behaviour of loose silty sand. Moreover, at the same fines fraction, the undrained shear strength in moist tamping method was found to be lower than that in dry tamping method, indicating the high collapsibility in specimen created by moist tamping method.

6. Microstructural observations

Fig. 9a and Fig. 9b display the microstructural observations of silty sand stacked up in dry state at two fines fractions of 5% and 10%, in which the black/white/blue regions graphically represent the inter-sand voids (black), the stacked up C500 silt (white) and the coloured HN31 sand (blue), respectively.

318 It can be observed from two images that the added fine particles not only filled the inter-sand voids,
319 but also located nearby the sand-sand contact points by separating them [44]. In that case, the host
320 sand was placed in a regular manner, forming a relatively stable internal voids system. The results in
321 Fig. 9a and Fig. 9b could further explain why the maximum void ratio e_{max} determined on air-dried
322 composite soil nonlinearly increased with fines fraction (see Fig. 2): (i) there was always an increasing
323 number of fine particles stuck between host sand, leading to the sustaining loosening of the overall soil
324 structure; consequently, the e_{max} rapidly increased with the addition of fine particles; (ii) with the
325 addition of fine particles before TFC (about 19%), still a little fine particles filled the inter-sand voids,
326 leading to the slow increase of e_{max}. On the contrary, in the case of fines fraction higher than TFC, the
327 inter-sand voids were expected to be fully filled up with fines, leading to the fast increase of e_{max}.
328 Similarly, Fig. 10a and Fig. 10b show the microstructural observations for silty sand prepared by moist
329 tamping method at fines fractions of 5% and 10%, respectively. It appears from the two figures that: (i)
330 fines were bulked together, and this phenomenon became more pronounced as fines fraction increased;
331 (ii) the coarse sand was covered by the bulked fines [15] with very few fines falling in the inter-sand
332 voids, which might be attributed to the capillary force while employing moist tamping method; (iii)
333 the coarse sand with the fines were generally in contact with each other, and the initial fabric of this
334 composite soil was irregular and primarily governed by aggregated coarse sand forming large
335 metastable macropores in such a loose state. This observed metastable structure for silty sand mixtures
336 is similar to that in clean sand specimen that was previously defined as “bulked sand” or “honeycomb-
337 structure” by Casagrande [11].

338

339 ## 7. Discussion

340 As regards the impact of fine particles observed in this study, the undrained shear resistance decreased
341 as the fines fraction increased by employing dry tamping method, while a total reversed phenomenon
342 was observed in the case of moist tamping method. Moreover, at the same fines fraction, the undrained
343 shear resistance in dry tamping method was found to be higher than that in moist tamping method.
344 Obviously, the different phenomena in the former might be attributed to the different roles of fines,

345 while in the latter might be due to the different soil arrangements created by two preparation methods
346 since all other controlled factors in the experimental procedure (e.g., I_{Dmat}, $\dot{\sigma}_c$ and I_p of fines employed)
347 were kept exactly identical.

348 For a clear exposition, representation of different structures of silty sand created by dry and
349 moist tamping methods are shown in Fig. 11 and Fig. 12, where large hollow and small solid circles
350 represent the host sand and the silt grains, respectively. In the case of silty sand reclaimed by dry
351 tamping in Fig. 11, the silt particles not only (i) fill the inter-sand voids, but also (ii) locate nearby the
352 sand-sand contact points by separating them since the mean diameter of C500 silt is about 6 μm, being
353 far smaller than that of host HN31 sand (350 μm). In the former case, the fine particles make no actual
354 mechanical contribution to the soil response and could be viewed as inactive since they are totally free
355 to shift. This is consistent with the conclusion drawn by Finn [45] that liquefaction brittleness is
356 irrespective of fine particles completely accommodated within inter-sand voids. In the latter case,
357 these silt particles initially loosen the host sand grains by separating them and facilitate the contractive
358 sliding of host sand [25] as well as inhibit the dilatant response when subjected to an imposed shearing
359 effort, especially in such a loose state (I_{Dmat}=0.00). And this weakening effect could be expected to be
360 much conspicuous at higher fractions. As a result, the deviator stress decreased with the increase of
361 fines fraction, as shown in Fig. 7a. As for overall host sand structure, the regularly placed soil fabric
362 (as compared with "metastable" macropores that presents in the moist tamping method in Fig. 10)
363 normally promotes an overall stable behavior and the limited quantity of silt grains in this study
364 (F_c<15%) could not sufficiently suppress the inherent dilatant tendency of this stable structure. Soon
365 after shearing, the silt grains in the latter case (weakening) commence to fall into inter-sand voids.
366 Concurrently, the host sand grains come into firmer contact with each other [32] and the weakening
367 effect of silt grains becomes much less important as loading continues. It should be also noted that (i)
368 the relatively low confining pressure (100 kPa) used in the present work normally supports a more
369 dilatant tendency [17,37]; (ii) the adoption of density index of sand matrix (or skeleton void ratio)
370 ensures that the degradation of host sand matrix due to the addition of fine particles (as compared with

371 the global void ratio) cannot occur as explained in the foregoing section. By combining the above
372 reasonings, a global strain-hardening response identified in Fig. 7a could then be expected.

373 In the case of silty sand reclaimed by moist tamping depicted in Fig. 12, the presence of
374 macropores (or large inter-sand voids) makes the composite soil exhibiting an extremely high
375 collapsibility potential and these macropores tend to decrease in volume upon loading, leading to more
376 generation of excess pore water pressure under undrained condition, as compared with that
377 reconstituted by dry tamping method. Subsequently, the overall soil becomes prone to liquefaction [6].
378 This could be the reason why composite silty sand reconstituted in submerged state exhibits a more or
379 less strain-softening response, as clearly identified by Fig. 8a. It is worth noting that, the silt particles
380 attached to the sand surface created during the preparation of specimen may fall into the inter-sand
381 voids due to the disappearance of capillary force after saturating. Due to the inherent limitation of
382 high-resolution optical microscope, it seems impossible to obtain the photo for fully saturated silty
383 sand (with back pressure) prior to shearing. However, it does not alter the fact that the metastable
384 structure could be weakened with the increase in silt particles due to the following two factors: (i) in
385 the initial state, the mechanical property of sand matrix is kept almost constant (sand grains still in
386 contact) even with the presence of fine particles since they are mostly attached to host sand; (ii) during
387 the saturation phase, the filling of large inter-sand voids (macropores) becomes increasingly more
388 important, mitigating the collapsibility of macropore. From a macro perspective, this weakening effect
389 owing to the addition of silt particles on metastable structure (or the clog of inter-sand voids) could
390 also be justified in triaxial conditions by: (i) the moderated decline tendency of deviator stress (see Fig.
391 8a) with axial strain after a peak value of deviator stress; (ii) the inhibited generation of excess pore
392 water pressure (see Fig. 8b) at small axial strain range, at which the soil structure could be represented
393 by the initial one. Moreover, during shearing, host coarse sand tends to contract each other; they could
394 possibly slide over the residual small-size silt particles surrounding them [18]. This fines-induced
395 separating effect favours, in particular, the dilatant movement between two successive sand grains,
396 leading to more rapid dissipation of Δu at higher fines fraction (see Fig. 8b).

According to the above analysis, it could be logically deduced that if the large inter-sand voids (forming the metastable structure) created in the moist tamping method are totally filled up with silt particles, the static liquefaction would not occur. In that case, the deviator stress obtained in the moist tamping would be very close to that in the dry tamping method. To verify this point, the q_{max} against the total fines fraction (F_c^{Tot} in Table 2) of silty sand specimens reclaimed by two methods is schematized in Fig. 13. It is worth noting that to compare with the evolution of e_{min} with F_c^{Tot} in Fig. 2, the total fine fraction F_c^{Tot} is used in Fig. 13 as comparison basis. It can be observed that q_{max} linearly increased in moist tamping method and decreased in dry tamping method. By fitting with two straight lines, a critical value F_c^{Tot} of about 21% was obtained at the intersection point, which is in good agreement with the TFC (approximately 19%) determined on air-dried sand-fines mixture, as shown in Fig. 2. This confirms that the large inter-sand voids forming the metastable structure was the main reason why liquefaction collapsibility was observed in the specimen prepared by moist tamping, and this metastable structure could be further gradually weakened by the addition of silt particles, characterized by the filling of large inter-sand voids.

It is worth noting that the above mechanism may not be appropriate for the following cases: (i) with higher fines fraction (F_c^{Tot}>TFC) while the global void ratio is used as comparison basis; (ii) dense silty sand specimen; (iii) with the addition of highly expansive clayey fines. In the first case, a decrease in undrained shear resistance with the addition of fines (e.g., fines fractions exceeded 30%) was reported by Erten [46] while using moist tamping method. This could be explained by the degradation of sand matrix. During the reconstitution stage, in order to keep global void ratio unchanged, the addition of fines significantly reduced the quantity of sand matrix (see Fig. 3a and 4a) providing the main shear resistance, and this adverse phenomenon became increasingly conspicuous at higher fines fraction, which certainly weakened the global granular structure. In the second case, Wood [26] performed undrained compression tests on Nevada Sand containing non-plastic silt and revealed that the effect of specimen preparation on the shear strength was negligible for specimens at higher densities. This may be attributed to the disappearance of metastable structure formed in the submerged state. In the last case, by examining sandy specimens with the addition of natural fines and

bentonite (e.g., I_p=98) reclaimed by moist tamping method, Abedi [47] reported that increasing a small amount of fines fraction made the specimens to sustain more instability in the small range of fines fraction. This phenomenon could be explained by the following two independent factors: (i) even with a small amount of water in moist tamping method, the clayey fine particles such as bentonite were highly sensitive to stick together and created aggregated structure, which rendered composite specimen non-uniform; (ii) swelling pressure generated from bentonite during the saturation phase introduced a non-negligible change of $\dot{\sigma}_c$. To the authors' knowledge, this variation linking to the addition of highly expansive fines remains an open question, and more studies are still needed.

Conclusion

In this study, the effect of two tamping-based specimen preparation methods was assessed using loose silica sand matrix containing various amounts of non-plastic silt, and by performing a series of undrained triaxial compression tests. For further analysis, microstructural observations were also conducted on loose silty sand specimens. The results obtained allow the following conclusions to be drawn:

1. When employing dry tamping method, the overall granular structure is very regular exhibiting a strong dilatant behaviour. In the case of mean diameter of silt being much smaller than that of host sand, there are always some parts of silt particles stuck between the adjacent sand grains, facilitating the relative contractive sliding of loose host sand. As a result, the deviator stress decreased as the silt fraction increased, exhibiting much less strain-hardening response.
2. When employing moist tamping method, due to the presence of large inter-sand voids forming the metastable structure, liquefaction collapsibility was observed. With the addition of silt particles, this metastable structure was weakened, characterized by the filling of large inter-sand voids, leading to the increase of liquefaction resistance.

Acknowledgements

The financial support provided by the research sponsors through ANR ISOLATE is gratefully acknowledged. The assistance of Madame Vue (Navier/Multi-échelle) with machining related to optical microscope is also gratefully acknowledged.

Reference

[1] Castro J. Liquefaction of sands. Ph.D Thesis Harvard Soil Mechanics Series n81, Cambridge, MA, 1969.

[2] Canou J. Contribution à l'étude et à l'évaluation des propriétés de liauéfaction d'un sable. Ph.D Thesis Ecole Nationale des Ponts et Chaussées, 1989.

[3] Ishihara K. Liquefaction and flow failure during earthquakes. Geotechnique 1993;43:351–451. https://doi.org/10.1680/geot.1993.43.3.351.

[4] Been K, Jefferies M. A state parameter for sands. Geotechnique 1985;35:99–112.

[5] Zhu Z, Cheng W. Parameter Evaluation of Exponential-Form Critical State Line of a State-Dependent Sand Constitutive Model. Appl Sci 2020;10:328. https://doi.org/10.3390/app10010328.

[6] Benahmed N, Canou J, Dupla JC. Structure initiale et propriétés de liquéfaction statique d'un sable. Comptes Rendus - Mec 2004;332:887–94. https://doi.org/10.1016/j.crme.2004.07.009.

[7] Mulilis J, Seed H, Chan C, Mitchell M, Arulanandan K, Asce M. Effects of sample preparation on sand liquefacton. J Geotech Geoenvironmental Eng 1977;103:91–108.

[8] Ladd R. Preparing test specimens using undercompaction. Geotech Test J 1978;1:16–23.

[9] Zlatovic S, Ishihara K. Normalized behavior of very loose non-plastic soils:effects of fabric. Soils Found 1997;37:47–56.

[10] Frost JD, Park JY. A critical assessment of the moist tamping technique. Geotech Test J 2003;26:57–70. https://doi.org/10.1520/gtj11108j.

[11] Casagrande A. Liquefaction and cyclic deformation of sands- A critical review. Cambridge, Mass: 1976.

[12] Tokimatsu K, Yoshimi Y. Empirical Correlation of Soil Liquefaction Based on SPT N-Value and Fines Content. Soils Found 1983;23.

[13] Shengcong F, Tatsuoka F. Soil Liquefaction During Haicheng and Tangshan Earthquake in China; A Review. Soils Found 1984;24:22–9.

[14] Amini F, Qi G. Liquefaction Testing of Stratified Silty Sands. J Geotech Geoenvironmental Eng 2000;126:208–17.

[15] Pitman T, Robertson P, Sego D. Influence of fines on the collapse of loose sands. Can Geotech J 1994;31:728–39.

[16] Benahmed N, Nguyen TK, Hicher PY, Nicolas M. An experimental investigation into the effects of low plastic fines content on the behaviour of sand/silt mixtures. Eur J Environ Civ Eng 2015;19:109–28. https://doi.org/10.1080/19648189.2014.939304.

[17] Jradi L. Study of the Influence of Fine Particles on the Properties of Liquefaction of Sands. Ph.D Thesis University Paris-Est, 2018.

[18] Zhu Z, Dupla J, Canou J, Foerster E. Experimental study of liquefaction resistance : effect of non-plastic silt content on sand matrix. Eur J Environ Civ Eng 2020;0:1–19. https://doi.org/10.1080/19648189.2020.1765198.

[19] Belkhatir M, Arab A, Della N, Missoum H, Schanz T. Liquefaction resistance of Chlef river silty sand: Effect of low plastic fines and other Parameters. Acta Polytech Hungarica 2010;7:119–37.

[20] Stamatopoulos CA. An experimental study of the liquefaction strength of silty sands in terms of the state parameter. Soil Dyn Earthq Eng 2010;30:662–78. https://doi.org/10.1016/j.soildyn.2010.02.008.

[21] Cherif Taiba A, Belkhatir M, Kadri A, Mahmoudi Y, Schanz T. Insight into the Effect of Granulometric Characteristics on the Static Liquefaction Susceptibility of Silty Sand Soils. Geotech Geol Eng 2016;34:367–82. https://doi.org/10.1007/s10706-015-9951-z.

[22] Papadopoulou AI, Tika TM. The effect of fines plasticity on monotonic undrained shear strength and liquefaction resistance of sands. Soil Dyn Earthq Eng 2016;88:191–206.

https://doi.org/10.1016/j.soildyn.2016.04.015.

[23] Yang J, Wei LM. Collapse of loose sand with the addition of fines: The role of particle shape. Geotechnique 2012;62:1111–25. https://doi.org/10.1680/geot.11.P.062.

[24] Eseller-Bayat EE, Monkul MM, Akin Ö, Yenigun S. The Coupled Influence of Relative Density, CSR, Plasticity and Content of Fines on Cyclic Liquefaction Resistance of Sands. J Earthq Eng 2019;23:909–29. https://doi.org/10.1080/13632469.2017.1342297.

[25] Zhu Z, Zhang F, Dupla JC, Canou J, Foerster E. Investigation on the undrained shear strength of loose sand with added materials at various mean diameter ratios. Soil Dyn Earthq Eng 2020;137. https://doi.org/10.1016/j.soildyn.2020.106276.

[26] Wood FM, Yamamuro JA, Lade P V. Effect of depositional method on the undrained response of silty sand. Can Geotech J 2008;45:1525–37. https://doi.org/10.1139/T08-079.

[27] Yamamuro JA, Wood FM, Lade P V. Effect of depositional method on the microstructure of silty sand. Can Geotech J 2008;45:1538–55. https://doi.org/10.1139/T08-080.

[28] Cubrinovski M, Ishihara K. Maximum and Mimimum Void Ratio Characteristics of Sands. Soils Found 2002;42:65–78.

[29] Xenaki VC, Athanasopoulos GA. Liquefaction resistance of sand-silt mixtures: An experimental investigation of the effect of fines. Soil Dyn Earthq Eng 2003;23:1–12. https://doi.org/10.1016/S0267-7261(02)00210-5.

[30] Zlatović S, Ishihara K. On the influence of nonplastic fines on residual strength. First Int. Conf. Earthq. Geotech. Eng., 1995, p. 239–44.

[31] Dang Q, REIFFSTECK P. Influence of plastic fines on the static liquefaction of sand. Jounées Nqtionqles de Géotechnique et de Géologie de l'Ingénieur 2018:1–8.

[32] Lade P, Yamamuro J. Effects of nonplastic fines on static liquefaction of sands. Can Geotech J 1997;34:918–28. https://doi.org/10.1139/t97-052.

526 [33] Monkul MM, Yamamuro JA. Influence of silt size and content on liquefaction behavior of
527 sands. Can Geotech J 2011;48:931–42. https://doi.org/10.1139/t11-001.

528 [34] Porcino DD, Diano V. The influence of non-plastic fines on pore water pressure generation and
529 undrained shear strength of sand-silt mixtures. Soil Dyn Earthq Eng 2017;101:311–21.
530 https://doi.org/https://doi.org/10.1016/j.soildyn.2017.07.015.

531 [35] Ishihara K, Kawase Y, Nakajima M. Liquefaction characteristics of sand deposits at an oil tank
532 site during the 1978 Miyagiken-Oki earthquake. Soils Found 1980;20:97–111.

533 [36] El Dine BS, Dupla JC, Frank R, Canou J, Kazan Y. Mechanical characterization of matrix
534 coarse-grained soils with a large-sized triaxial device. Can Geotech J 2010;47:425–38.
535 https://doi.org/10.1139/T09-113.

536 [37] Benahmed N. Comportement mécanique d'un sable sous cisaillement monotone et cyclique:
537 application aux phénomènes de liquéfaction et de mobilité cyclique. Ph.D Thesis Ecole
538 Nationale Des Ponts et Chaussées, 2001.

539 [38] Polito P, Martin R. Effects of nonplastic fines on the liquefaction resistance of sands. J Geotech
540 Geoenvironmental Eng 2001;127:408–15.

541 [39] Dash HK, Sitharam TG. Undrained monotonic response of sand-silt mixtures: Effect of
542 nonplastic fines. Geomech Geoengin 2011;6:47–58.
543 https://doi.org/10.1080/17486021003706796.

544 [40] Kuerbis R, Vaid Y. Sand sample preparation-the slurry deposition method. Soils Found
545 1988;28:107–18.

546 [41] Yamamuro J, Covert K. Monotonic and cyclic liquefaction of very loose sands with high silt
547 content. J Geotech Geoenvironmental Eng 2001;127:314–24.

548 [42] Carraro JAH, Prezzi M. A new slurry-based method of preparation of specimens of sand
549 containing fines. Geotech Test J 2008;31:1–11. https://doi.org/10.1520/GTJ100207.

550 [43] Vaid YP, Sivathayalan S, Stedman D. Influence of Specimen-Reconstituting Method on the

551 Undrained Response of Sand. Geotech Test J 1999;22:187–95.
552 https://doi.org/10.1520/gtj11110j.

553 [44] Monkul MM, Etminan E, Şenol A. Coupled influence of content, gradation and shape
554 characteristics of silts on static liquefaction of loose silty sands. Soil Dyn Earthq Eng
555 2017;101:12–26. https://doi.org/10.1016/j.soildyn.2017.06.023.

556 [45] Finn WD, Ledbetter RH, Wu G. Liquefaction in silty soils: design and analysis. Liq. silty soils
557 Des. Anal. Gr. Fail. under Seism. Cond., 1994, p. 51–76.

558 [46] Erten D, Maher MH. Cyclic undrained behavior of silty sand. Soil Dyn Earthq Eng
559 1995;14:115–23. https://doi.org/10.1016/0267-7261(94)00035-F.

560 [47] Abedi M, Yasrobi SS. Effects of plastic fines on the instability of sand. Soil Dyn Earthq Eng
561 2010;30:61–7. https://doi.org/10.1016/j.soildyn.2009.09.001.

562

563 Figures and Tables

564 Figure 1 Grain size distribution curves for HN31 sand and non-plastic C500 silt

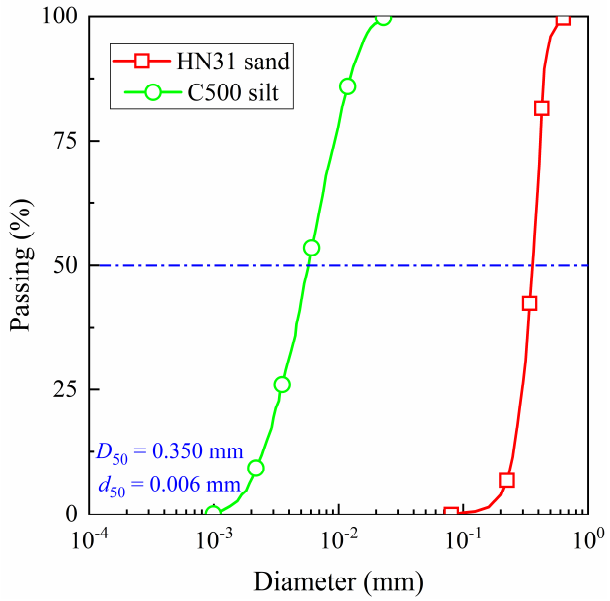

565

566

567

568

569

570

571

572 Figure 2 Evolution of maximum and minimum void ratios of HN31-C500 mixtures with the addition
573 of C500 silt (after [18])

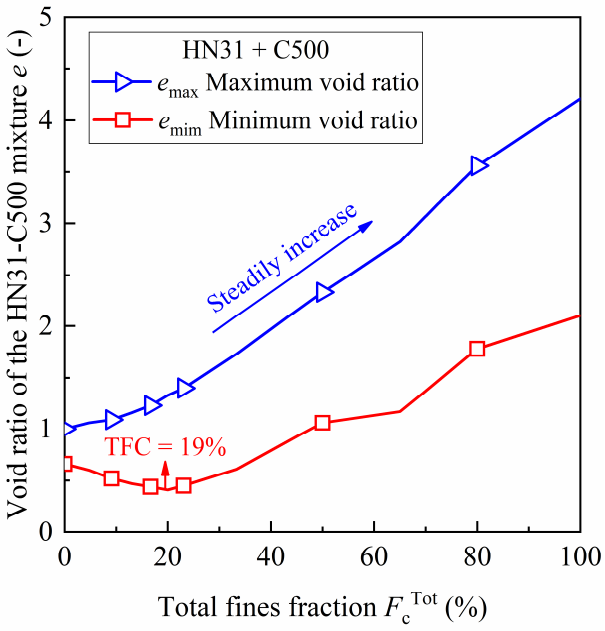

574

575

576

577

578

579

580

581

582

583

584

585

586

587 Figure 3 Configurations of sand containing fines: (a) sand-dominance (F_c^{Tot}<TFC); (b) fines-
588 dominance (F_c^{Tot}>TFC) (after [18])

(a) sand-dominance

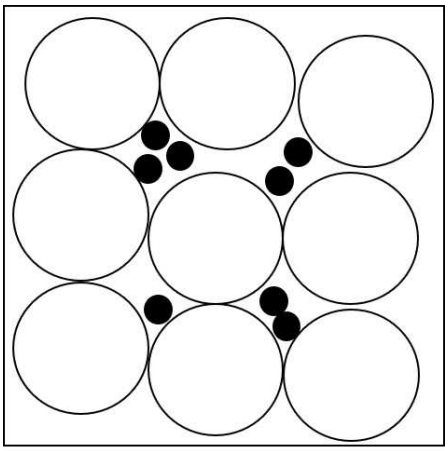

F_c^{Tot}<TFC

(b) fines-dominance

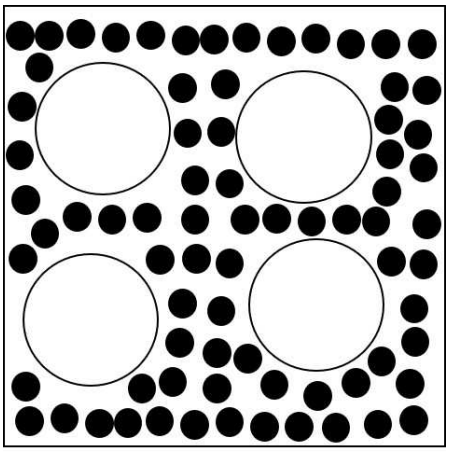

F_c^{Tot}>TFC

589

590

591

592

593

594

595

596

597

598

599

600

601

602 Figure 4 Concept of (a) constant sand matrix; (b) constant global void ratio (from [25])

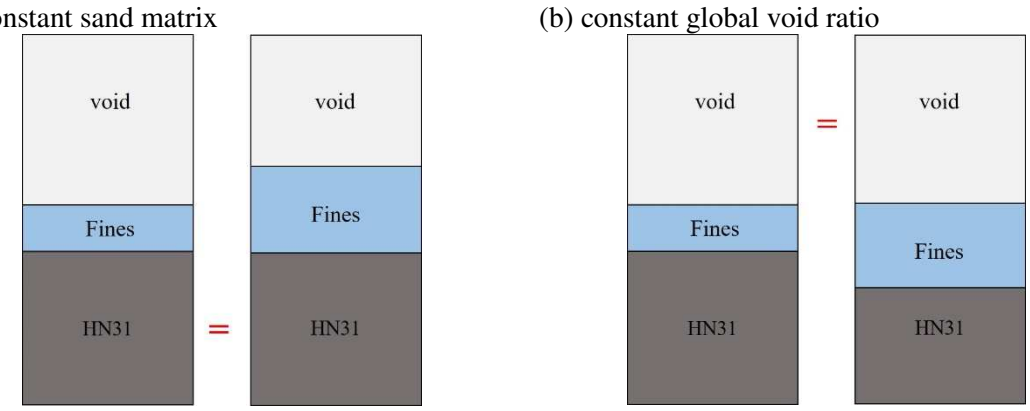

603

604

605

606

607

608

609

610

611

612

613

614

615

616

617

618 Figure 5 HN31 sand coloured by Basacid Blue 762 liquid

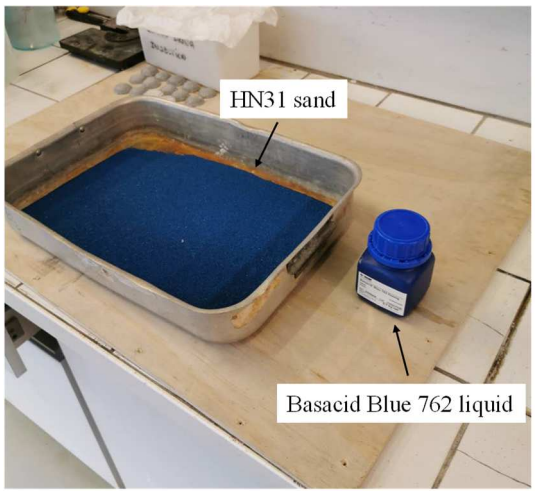

619

620

621

622

623

624

625

626

627

628

629

630

631

632

633

634 Figure 6 (a) Silty sand specimen with coloured HN31 sand; (b) high-resolution optical microscope

(a) (b)

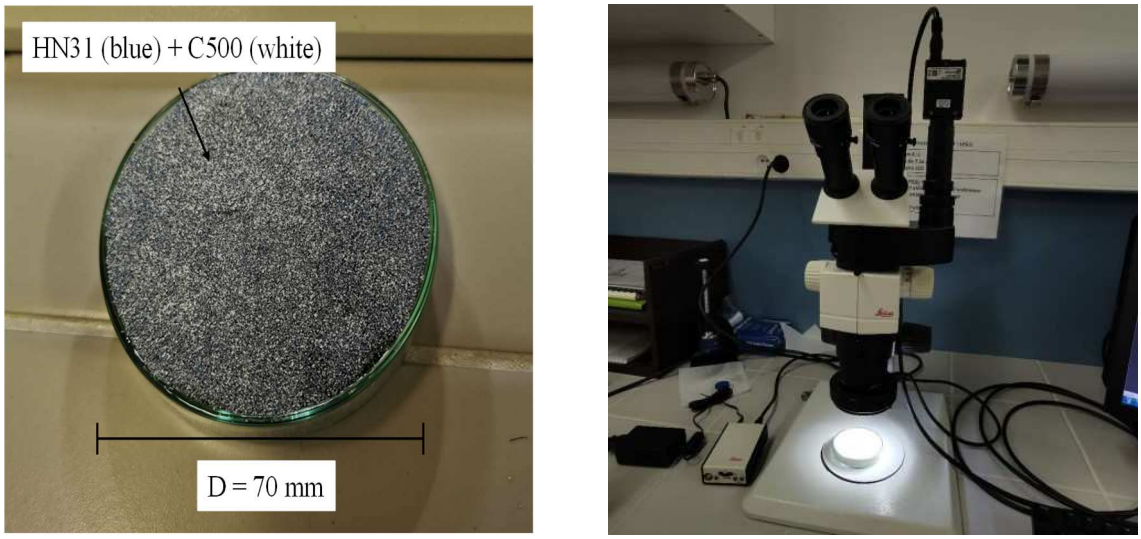

635

636

637

638

639

640

641

642

643

644

645

646

647

Figure 7 Triaxial test results of silty sand specimens in very loose state at various fines fractions of confining pressure equalling to 100 kPa reclaimed by dry tamping: (a) deviator stress against axial strain; (b) excess pore water pressure against axial strain (from [25])

(a) (b)

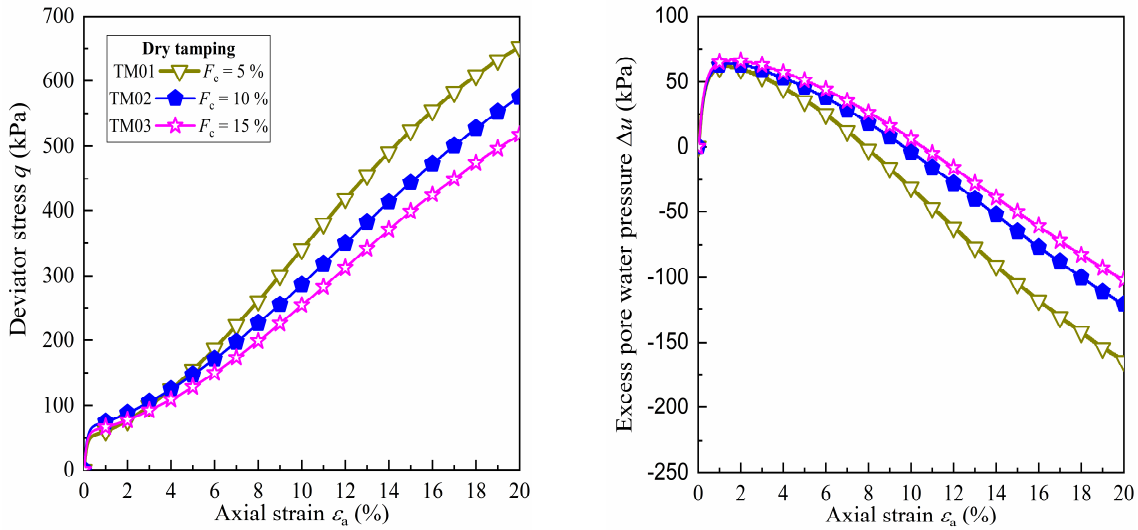

Figure 8 Triaxial test results of silty sand specimens in very loose state at various fines fractions of confining pressure equalling to 100 kPa reclaimed by moist tamping: (a) deviator stress against axial strain; (b) excess pore water pressure against axial strain (from [18])

(a) (b)

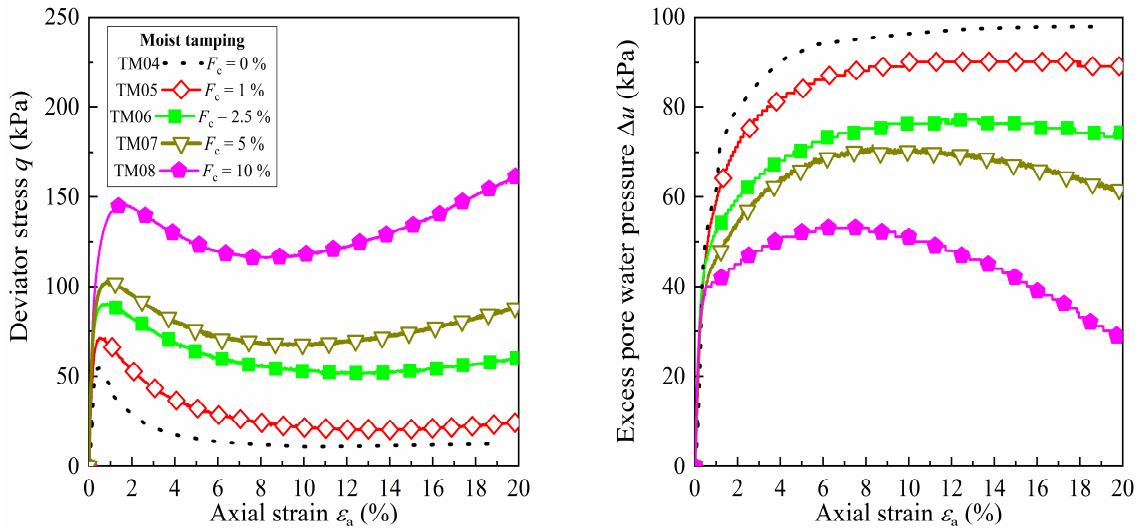

679 Figure 9 Microstructural observations of silty sand specimens in very loose state reclaimed by dry
680 tamping at (a) F_c=5%; (b) F_c=10%

(a) (b)

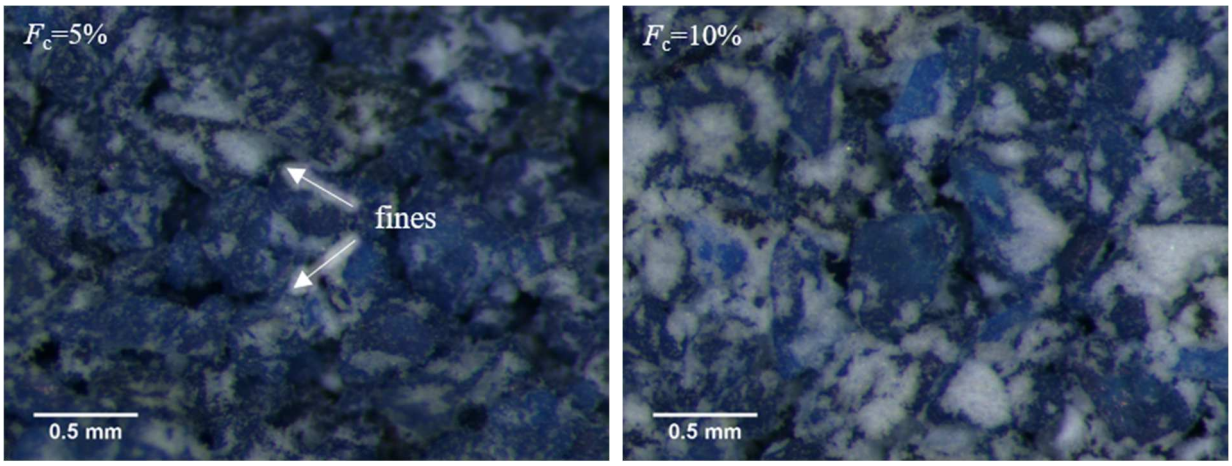

681

682

683

684

685

686

687

688

689

690

691

692

693

694

695 Figure 10 Microstructural observations of silty sand specimens in very loose state reclaimed by moist
696 tamping at (a) F_c=5%; (b) F_c=10%

(a) (b)

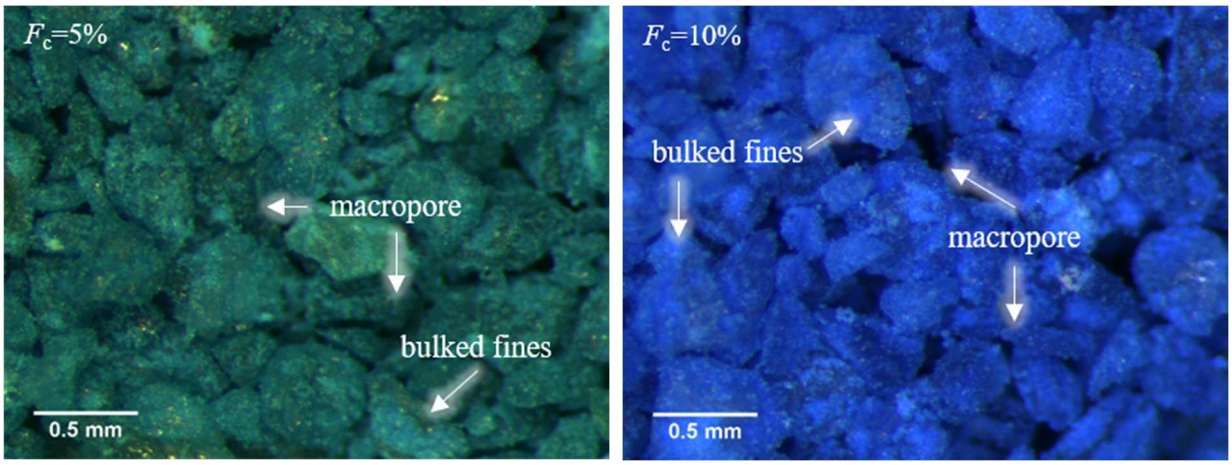

697

698

699

700

701

702

703

704

705

706

707

708

709

710

Figure 11 Schematic diagram of hypothesized silty sand fabric reconstituted by dry tamping

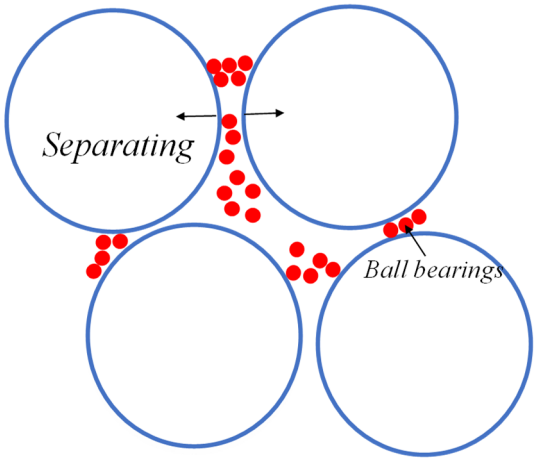

728 Figure 12 Schematic diagram of hypothesized silty sand fabric reconstituted by moist tamping

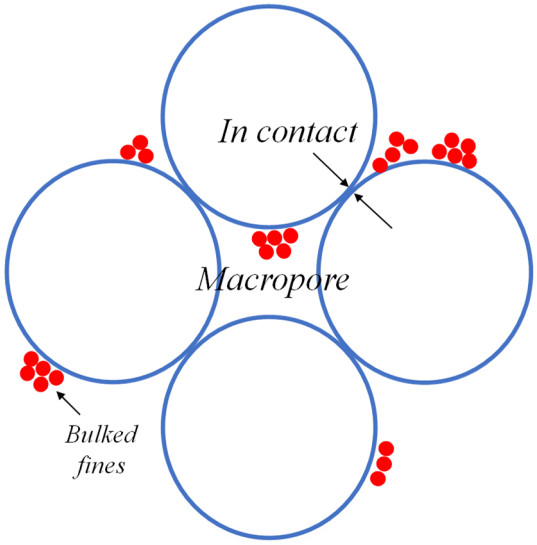

729

730

731

732

733

734

735

736

737

738

739

740

741

742

743 Figure 13 Evolution of peak deviator stress against total fines fraction

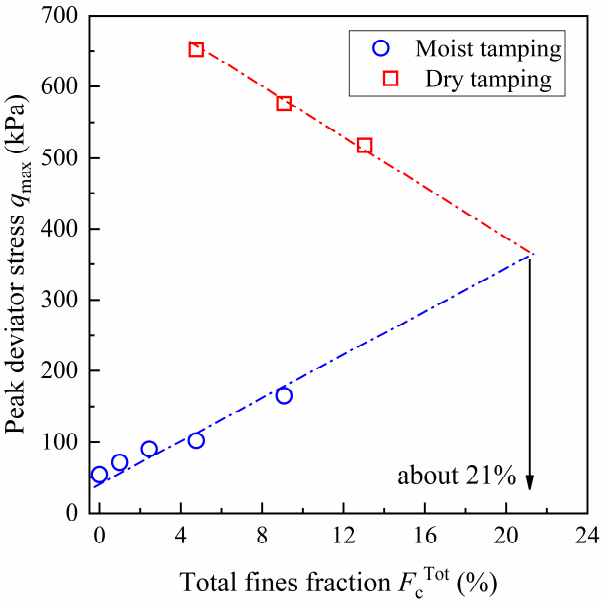

744

745

746

747

748

749

750

751

752

753

754

755

756

757

758 Table 1 Index properties of test materials

Material	D_{50} or d_{50} (μm)	D_{10} or d_{10} (μm)	C_u	e_{min}	e_{max}	G_s	I_p
HN31	350	250	1.57	0.656	1.00	2.65	NP (non-plastic)
C500	6	2	3.15	-	-		

759

760

761

762

763
764

765

766

767

768

769

770

771

772

773

774

775

776

777 Table 2 Details of triaxial tests programme

Reference	F_c (%)	F_c^{Tot} (%)	Depositional method	I_{Dmat}	σ'_c (kPa)
TM01	5.0	4.8	D[(i)]	0.00	100
TM02	10.0	9.1	D		
TM03	15.0	13.0	D		
TM04	0.0	0.0	M[(ii)]		
TM05	1.0	1.0	M		
TM06	2.5	2.4	M		
TM07	5.0	4.8	M		
TM08	10.0	9.1	M		
Note	D[(i)]: Dry tamping M[(ii)]: Moist tamping				

778